HHS Public Access

Author manuscript

Brain Behav Immun. Author manuscript; available in PMC 2016 July 01.

Published in final edited form as:

Brain Behav Immun. 2016 July ; 55: 82–92. doi:10.1016/j.bbi.2015.11.007.

Microglial P2Y12 Receptors Regulate Microglial Activation and Surveillance during Neuropathic Pain

Nan Gu[1,2,#], **Ukpong B. Eyo**[2,#], **Madhuvika Murugan**[2], **Jiyun Peng**[2], **Sanjana Matta**[2], **Hailong Dong**[1,*], and **Long-Jun Wu**[2,*]

[1]Department of Anesthesiology, Xijing Hospital, Fourth Military Medical University, Xi'an, Shaanxi Province, PR China 710032

[2]Department of Cell Biology and Neuroscience, Rutgers University, Piscataway, NJ, USA 08854

Abstract

Microglial cells are critical in the pathogenesis of neuropathic pain and several microglial receptors have been proposed to mediate this process. Of these receptors, the P2Y12 receptor is a unique purinergic receptor that is exclusively expressed by microglia in the central nervous system (CNS). In this study, we set forth to investigate the role of P2Y12 receptors in microglial electrophysiological and morphological (static and dynamic) activation during spinal nerve transection (SNT)-induced neuropathic pain in mice. First, we found that a genetic deficiency of the P2Y12 receptor ($P2Y12^{-/-}$ mice) ameliorated pain hypersensitivities during the initiation phase of neuropathic pain. Next, we characterized both the electrophysiological and morphological properties of microglia in the superficial spinal cord dorsal horn following SNT injury. We show dramatic alterations including a peak at 3 days post injury in microglial electrophysiology while high resolution two-photon imaging revealed significant changes of both static and dynamic microglial morphological properties by 7 days post injury. Finally, in $P2Y12^{-/-}$ mice, these electrophysiological and morphological changes were ameliorated suggesting roles for P2Y12 receptors in SNT-induced microglial activation. Our results therefore indicate that P2Y12 receptors regulate microglial electrophysiological as well as static and dynamic microglial properties after peripheral nerve injury, suggesting that the microglial P2Y12 receptor could be a potential therapeutic target for the treatment of neuropathic pain.

Keywords

Microglia; P2Y12 Receptor; Neuropathic Pain; Electrophysiology; Surveillance; 2-photon imaging

[*]**Correspondence:** Dr. Long-Jun Wu, Dept. of Cell Biology and Neuroscience, Rutgers University, Room B333 Nelson Labs, Piscataway, NJ 08854, TEL: (732) 445-2182; FAX: (732) 445-5870, lwu@dls.rutgers.edu, Dr. Hailong Dong, Department of Anesthesiology, Xijing Hospital, Fourth Military Medical University, Changle West Rd 127, Xi'an, Shaanxi 710032, China. hldong6@hotmail.com.

[#]equal contribution

Conflict of Interest: The authors declare no competing financial interests.

1. INTRODUCTION

Neuropathic pain is a condition in which, following an initial injury to the somatosensory nervous system, non-physiological pain develops that is characterized by hyperalgesia, allodynia and spontaneous pain. Therapies for neuropathic pain based on neurocentric mechanisms have not been entirely effective in its treatment and require alternative approaches (Baron, 2006; Gu et al., 2012). Glial cells of the central nervous system (CNS) have received increasing attention in the pathological mechanisms underlying the development of such pain conditions (Liu and Yuan, 2014; Old et al., 2015; Vallejo et al., 2010). Specifically, microglia, the immunocompetent cells of the CNS, are activated following peripheral nerve injury and promote neuropathic pain through releasing various factors, such as pro-inflammatory mediators, ROS, and BDNF (Clark et al., 2013; Ferrini and De Koninck, 2013; Inoue and Tsuda, 2012; Kim et al., 2010). However, the molecular mechanism underlying nerve injury-induced microglial activation in the spinal dorsal horn remains largely unknown and a better understanding of microglial mechanisms of neuropathic pain development are required.

Microglial purinergic receptors, including metabotropic P2Y12 receptors and ionotropic P2X4 and P2X7 receptors, have been implicated in the pathogenesis of neuropathic pain (Trang et al., 2012; Tsuda et al., 2013). Although extensive work has been carried out on P2X4 and P2X7 regulation of microglial phenotypes and function during neuropathic pain, there has been less understanding of the contribution of P2Y12 receptors to pain hypersensitivities. Moreover, unlike the ionotropic P2X receptors, P2Y12 receptors are exclusively expressed on microglia but not in other glial cells and neurons in the CNS. Previous studies have shown that both pharmacological (Kobayashi et al., 2008) and genetic (Tozaki-Saitoh et al., 2008) inhibition of microglial P2Y12 receptors improve pain phenotypes in rodents. Yet, whether these receptors control static and dynamic morphological properties and electrophysiological activities in microglia during the development of neuropathic pain is not known.

In the present study, employing a genetic approach in a spinal nerve transection (SNT) model, we first confirmed that $P2Y12^{-/-}$ mice displayed less pain phenotypes than WT mice. Next, whole-cell recording in microglia found dramatic electrophysiological activation, while high resolution two-photon imaging revealed that microglial processes retracted significantly with heightened dynamics following the SNT surgery. Finally, a genetic deficiency of the P2Y12 receptor reduced these SNT-induced microglial activation properties. These results indicate that P2Y12 receptors regulate microglial activation and thus may serve as a target to limit microglial activation and its detrimental consequences during neuropathic pain.

2. MATERIALS AND METHODS

2.1 Animals

Both male and female mice were used in accordance with institutional guidelines, as approved by the animal care and use committee at Rutgers University. All animals were housed under controlled temperature, humidity, and lighting (light: dark 12:12 hr. cycle)

with food and water available *ad libitum*. GFP reporter mice ($CX3CR1^{GFP/GFP}$) were purchased from the Jackson Laboratory (Jung et al., 2000). Heterozygous ($CX3CR1^{GFP/+}$) were used for all experiments as "wild type" controls by crossing homozygous ($CX3CR1^{GFP/GFP}$) GFP reporter mice that express GFP under control of the fractalkine receptor (CX3CR1) promoter with C57BL/6J mice. Although fractalkine signaling is known to contribute to pain hypersensitivities (Johnston et al., 2004; Staniland et al., 2010), no obvious haplogenic effects of $CX3CR1^{GFP/+}$ on neuropathic pain were found. $CX3CR1^{GFP/+}$ heterozygous and WT C57BL/6J mice generated similar SNT-induced pain phenotypes (Figure S1) and so all mice used for the current studies were on a $CX3CR1^{GFP/+}$ background to facilitate the visualization of GFP-expressing microglia. $P2Y12^{-/-}$ mice, generated on a C57BL/6J background (Andre et al., 2003), were originally donated by Dr. Michael Dailey at the University of Iowa and were crossed with homozygous ($CX3CR1^{GFP/GFP}$) mice to generate $P2Y12^{-/-}$; $CX3CR1^{GFP/+}$ mice. All genotype backgrounds of mice used were viable and showed no detectable developmental defects. Six- to 9-week-old age-matched $CX3CR1^{GFP/+}$ and $P2Y12^{-/-}$; $CX3CR1^{GFP/+}$ mice were used to conduct nerve injury and subsequent pain behavioral test, spinal cord two-photon in vivo imaging, or spinal cord two-photon slice imaging experiments.

2.2 Spinal Nerve Transection (SNT)

Mice were anesthetized with isoflurane in O_2 (induction: 4–5% isoflurane; maintenance: 1.5–2.5% isoflurane). Lumbar 4 spinal nerve transection (SNT) surgery was performed as previously described (Chung et al., 2004) with slight modifications. Briefly, a small incision to the skin overlaying L5-S1 was made, followed by retraction of the paravertebral musculature from the vertebral transverse processes. The L4 spinal nerve was identified, lifted slightly, transected, and removed 1–1.5 mm from the end to dorsal root ganglia (DRG). The wound was irrigated with saline and closed in with a two-layer suture by closing the muscles with 6–0 silk sutures and the skin with 5–0 silk sutures. The L4 spinal nerve was only exposed without ligation or transection in sham-operated mice.

2.3 Behavioral Tests

Mice were previously acclimated to the environment and the experimenter on three successive days just before the SNT or sham operation. The tests were performed in a quiet temperature-controlled (23 ± 1 °C) room between the hours of 9:00 and 12:00 A.M. on days before and 2, 3, 5, 7 days after the surgery.

Mechanical allodynia was determined by measuring the incidence of foot withdrawal in response to mechanical indentation of the plantar surface of each hind paw with a sharp, cylindrical probe with a uniform tip diameter of approximately 0.2 mm provided by a set of Von Frey filaments (0.04 – 2g; North Coast medical, Inc.) using a protocol similar to that described previously (Gu et al., 2012). In brief, the mouse was placed on a metal mesh floor and covered with a transparent plastic dome (10 X 15 X 15 cm). The animal rested quietly in this situation after an initial few (~15) minutes of exploration. Each filament was applied from underneath the metal mesh floor to the plantar surface of the foot. The duration of each stimulus was 3s, in the absence of withdrawal, and the interstimulus interval was 10–15s. The incidence of foot withdrawal was expressed as a percentage of the 10 applications of

each stimulus as a function of force. Fifty percent withdrawal threshold values were determined.

Thermal hyperalgesia was assessed by measuring foot withdrawal latency to heat stimulation using a protocol that we have described previously (Gu et al., 2012). An analgesia meter (Model 336TG, IITC Life Science, Inc.) was used to provide a heat source. In brief, each mouse was placed in a box containing a smooth, temperature-controlled glass floor (30°C) and allowed to habituate for 20 min. The heat source was focused on a portion of the hind paw, which was flush against the glass, and a radiant thermal stimulus was delivered to that site. The stimulus shut off when the hind paw moved (or after 6s to prevent tissue damage). The intensity of the heat stimulus was maintained constant throughout all experiments. The elicited paw movement occurred at a latency between 2.5 and 4s in control animals. Thermal stimuli were delivered four times to each hind paw at 5 to 6 min intervals.

2.4 Immunohistochemistry

Mice were deeply anesthetized with isoflurane (5% in O_2) and perfused transcardially with 30ml PBS followed by 30 ml of cold 4% paraformaldehyde (PFA) in PBS containing 1.5% picric acid. The spinal cord were removed and post-fixed with the same 4% PFA overnight at 4°C. The samples were then transferred to 30% sucrose in PBS for 48 hr. Sample sections (20 μm in thickness) were prepared on gelatin-coated glass slide with a cryostat (Leica). The sections were blocked with 5% goat serum and 0.3% Triton X-100 (Sigma) in TBS buffer for 60 min, and then incubated overnight at 4°C with primary antibody for rabbit-anti-P2Y12 (1:500, Anaspec Inc.). The sections were then incubated for 60 min at RT with secondary antibodies (Alexa Fluor® 594, Life Technologies). The sections were mounted with Fluoromount-G (SouthernBiotech) and fluorescent images were obtained with a confocal microscope (LSM510, Zeiss). Fluorescent signal intensity was quantified using ImageJ software (National Institutes of Health, Bethesda, MD).

To quantify P2Y12 immunoreactivity profiles in the spinal cord, three to five L4–5 spinal cord segments per mouse from 4 mice were randomly selected for each group. The P2Y12 immunoreactivity data in WT Sham tissues was set as the 100% baseline and the data from each of the other groups were normalized and compared with this sham data.

2.5 Spinal Cord Slice Preparation

Freshly isolated spinal cord slices were prepared from 6–8-week-old sham mice or mice with SNT-induced neuropathic pain at the stated time points. Briefly, mice were deeply anesthetized with isoflurane, and lumbosacral laminectomies were performed in an ice-cold chamber. The lumbosacral spinal cord was quickly removed and placed in ice-cold, sucrose-substituted artificial CSF saturated with 95% O_2 and 5% CO_2 (sucrose ACSF, in mM: sucrose, 234; KCl, 3.6; $CaCl_2$, 2.5; $MgCl_2$, 1.2; NaH_2PO_4, 1.2; $NaHCO_3$, 25; and D-glucose, 12). Transverse lumbar spinal cord slices (300μm) were also prepared in ice-cold sucrose ACSF using a vibrating microtome. The slices were then maintained in a recovery chamber for 30 or more minutes at room temperature (23 ± 1°C) in regular ACSF equilibrated with 95% O_2 and 5% CO_2 (ACSF, in mM: NaCl, 125; KCl, 2.5; $CaCl_2$, 2;

$MgCl_2$, 1, NaH_2PO_4, 1.25; $NaHCO_3$, 26; and D-glucose, 25, and sucrose added to make 300–320 mOsmol) before imaging or electrophysiological studies.

2.6 Two-photon Imaging

2.6.1 Spinal Cord Slice Two-photon Imaging—Experiments were conducted at room temperature with slices maintained in oxygenated ACSF with the same composition as above in a perfusion chamber at a flow rate of 2 ml/min. GFP-labelled microglia, were typically imaged using a two-photon microscope (Scientifica Inc, UK) with a Ti:Sapphire laser (Mai Tai; Spectra Physics) tuned to 900nm with a 40X water immersion lens (0.8 NA; Olympus). Fluorescence was detected using a photomultiplier tube in whole-field detection mode and a 565 nm dichroic mirror with a 525/50 nm emission filter. The laser power was maintained at 25 mW or below and images were collected at between 40 and 80 μm from the slice surface. For imaging microglial dynamics, 20 consecutive z-stack images were collected at 1 μm intervals every minute and combined to make time-lapse movies. Microglia imaging was limited to a 3 hr. window after slicing to limit microglial activation effects in response to slicing as a confounding variable to data collection.

2.6.2 Spinal Cord In Vivo Two-photon Imaging—As described previously (Davalos et al., 2008), an anesthetic mix of ketamine-xylazine-acepromazine was used to anesthetize the mouse. The mouse was stabilized using a stabilizing spinal column, head, and tail custom-ordered clamps (model STS-A; Narishige) to minimize movement associated artifacts. After a T12-L1 laminectomy, the lumbar spinal cord was exposed at the L5 level. Under a binocular microscope with 8X to 40X magnification, the dura was cut and removed. A small well of Gelseal (Amersham Biosciences Corp.) was built around the exposed spinal cord to facilitate the maintenance of the tissue in a drop of artificial cerebrospinal fluid (ACSF) and for the immersion of the microscope lens in this solution for *in vivo* imaging. As described above, we used a two-photon microscope (Scientifica Inc, UK) with a Ti:Sapphire laser (Mai Tai; Spectra Physics) tuned to 900nm for *in vivo* imaging (Eyo et al., 2015; Eyo et al., 2014). Images of the superficial dorsal horn were obtained by preparing image stacks (165 X 165 μm, 1 μm z steps) collected at a depth of 30–80 μm of the spinal surface. At the end of the experiments, the mice were given an overdose of anesthetic and then sacrificed by cervical dislocation.

2.7 Patch Clamp Recordings

Whole cell patch-clamp recordings were made from dorsal horn microglia located in laminar layers I-III of freshly excised spinal cord slices. GFP-labeled microglia were studied in voltage-clamp mode (Wu et al., 2012). After establishing the whole-cell configuration, microglia were held at either −60 mV or −20mV. The resistance of a typical patch pipette was 4–6 MΩ. Recording electrodes contained a K^+-based internal solution composed of (in mM: 120 K-gluconate, NaCl, 5; $MgCl_2$, 1; EGTA, 0.5; MgATP, 2; Na_3GTP, 0.1; and HEPES, 10; pH 7.2; 280 –300 mOsmol). Membrane currents were amplified with an Axopatch 200B amplifier (Multiclamp 700B, Axon Instruments). Signals were filtered at 2 kHz and digitized (DIGIDATA 1440A), stored, and analyzed by pCLAMP (Molecular Devices, Union City, CA).The membrane capacitance (WT:27.02 ± 1.9 pF, and $P2Y12^{-/-}$: 22.76 ± 0.1 pF), the membrane resistance (WT: 1.41 ± 0.07 GΩ and $P2Y12^{-/-}$: 1.61 ± 0.17

GΩ), and the membrane potential (WT: −21.85 ± 1.74 mV, n=10 and P2Y12$^{-/-}$: −20.93 ± 1.26 mV) were noted. Data were discarded when the input resistance changed >20% during recording.

The diameter of the ATP application pipette tip was 3–4 μm. The pressure (10 psi) and duration (100 ms) of the puff was controlled and the distance between the patched cell and puff pipette was kept constant (~15 μm). This was achieved by marking the position of the two pipettes (recording and puff) on the display screen and adjusting the distance of the puff pipette until the preferred distance was reached.

2.8 Static Microglial Morphological Properties Quantification

To quantify GFP-positive cells profiles in the spinal cord, two to four L4–5 spinal cord segments per mouse from 4–5 mice were randomly selected. An image in a square (165 X 165 μm^2) centered on the superficial dorsal horn (laminas I–III) was captured, and all of the intact GFP-positively labeled cells in the frame were analyzed with ImageJ software (National Institutes of Health, Bethesda, MD). The data from several slices from different mice were analyzed and pooled to determine significance.

2.8.1 Process Length Analysis and End Point Voxel Analysis—A skeleton analysis method was developed to quantify microglia morphology from two-photon images as previously described (Morrison and Filosa, 2013) with slight modifications. Two-photon images (20 μm z-stack at 1 μm intervals) were acquired during 30 min imaging sessions in the ipsilateral and contralateral region as identified in Figure S2A–B. Two-dimensional (2D) stacked images were made using the ImageJ program. For skeleton analysis, the maximum intensity projection image of the GFP signal was de-speckled to eliminate background noise. The resulting image was converted to a binary image and skeletonized (Figure S2C). The Analyze Skeleton plugin (http://imagejdocu.tudor.lu/) was then applied to all skeletonized images to collect data on the number of endpoints per frame (Figure S2C, blue) and process length (Figure S2C, orange). With regards to the number of cells quantified for the microglial Process Length Analysis and End Point Voxel Analysis, we used all the cells in the field of view which ranged from ~40 total cells in control tissues to up to ~120 cells at POD7 after SNT. These data were used as measures of microglial morphology based on previous reports showing reduced microglia process branching complexity and process length during microglial activation (Fontainhas et al., 2011; Orr et al., 2009; Stence et al., 2001). The number of cell somas per frame was used to normalize all process endpoints and process lengths.

2.8.2 Sholl Analysis—For Sholl analysis, z-stacked two photon images (20 μm) were acquired at 1μm intervals. Consecutive z-stack images were converted to maximum intensity projection images using Image J software. Using the Image5D plugin, z-stack images were condensed into a maximum intensity projection images over which concentric circles were drawn (concentric circles plugin), centered on the soma, beginning at 7μm radii and increasing with every circle. Sholl analysis was manually performed for each cell by counting the number of intersections between microglial processes and each increasing circle to create a Sholl plot. Because of the nature of our imaging, a small field of view with

a few intact cells (3–5 cells) were quantified from each slice in ~5 mice for the Sholl analysis.

From these data we determined the process maximum (Nm, the maximum number of intersections), the critical radius (Cr, the distance at which the Nm occurred, reflecting sites of highest branch density), the maximum branch length (μm, the maximum radius at which a branch intersection occurred) and the number of primary branches (Np, the number of branches that originated from the microglia soma. Here, we used the number of intersections at starting radius). From these parameters, a Shoenen ramification index was calculated (Nm/Np) manually to quantify cell branching density.

2.9 Dynamic Microglial Process Motility Analysis

For in vivo imaging experiments, 4 (POD 7) and 6 (sham) mice were used and 6–11 slices from 3–6 mice were used for slice imaging experiments. Microglial process motility analysis was carried out as described previously (Eyo and Dailey, 2012). Briefly, 3D image stacks were combined to make 2D projection images for each time point. Then, to account for any *x*–*y* tissue drift, 2D projection images from the generated time lapse movies were registered using the StackReg plugin. Registered images were then smoothened to reduce background noise. To define the cell boundary, an arbitrary threshold was applied uniformly to all images in a given time sequence. To generate difference images, the absolute difference between two sequential thresholded images in a time series was calculated using the "Difference" tool of the "Image Calculator" feature of ImageJ. Sequential difference images in a time sequence were used to generate a motility index, which is a percent change in area of the cell at adjacent timepoints.

2.10 Statistical Analysis

All data are expressed as mean ± S.E.M. Changes of values of each experimental group were tested using Student's t-test or one way ANOVA, followed by individual post hoc comparisons (Fisher's exact test) to establish significance. Behavioral data were analyzed using unpaired Student's t test (compared different time points in any 2 groups) or Repeated Measures ANOVA followed by post-hoc Bonferroni test. A difference was accepted as significant if $P < 0.05$.

3. RESULTS

3.1 Upregulation of the Microglial P2Y12 Receptor and Its Role in Neuropathic Pain Hypersensitivities

The P2Y12 receptor is known to be specifically expressed in CNS microglia (Butovsky et al., 2014; Haynes et al., 2006; Zhang et al., 2014). Using $CX3CR1^{GFP/+}$ (henceforth referred to as "WT" for simplification) mice where microglia are labeled with GFP, we confirmed that P2Y12 expression completely overlaps with GFP and thus is exclusively expressed in microglia in the spinal cord (Figure 1A, Figure S3). After SNT surgery, the number of GFP-expressing microglia was largely increased in the ipsilateral dorsal horn (Figure 1A–B, Figure S4). In addition, P2Y12 immunoreactivity in the spinal cord was ~1.4 times and ~2.0 times significantly upregulated in the ipsilateral spinal cord dorsal horn at post-operative day

(POD) 3 and POD 7 following SNT surgery compared with that in WT Sham mice, respectively (n=4 mice per group. Figure 1A, C, Figure S4). No significant difference was found between WT sham group and the contralateral side at POD 3 and POD 7 following SNT surgery (Figure 1A, C). As expected, P2Y12 immunoreactivity was absent in $P2Y12^{-/-}$; $CX3CR1^{GFP/+}$ (henceforth referred to as "$P2Y12^{-/-}$") mice (Figure1B–C). Finally, we examined pain behaviors after SNT in WT and $P2Y12^{-/-}$ mice. Consistent with a previous report (Tozaki-Saitoh et al., 2008), we found that both thermal hyperalgesia (Figure 1D) and mechanical allodynia (Figure 1E) were reduced in $P2Y12^{-/-}$ mice at PODs 3, 5, and 7 following SNT surgery. Given the evidence of sex differences recently reported in established pain (Sorge et al., 2015), we performed experiments to compare pain phenotypes between male and female $P2Y12^{-/-}$ and WT mice. No obvious sex differences were found in the initiation phase (POD 1–7) of neuropathic pain after SNT surgery (Figure S5). These results indicate that the P2Y12 receptor is upregulated in spinal microglia and contributes to neuropathic pain hypersensitivities.

3.2 P2Y12 Receptors Contribute to Electrophysiological Activation of Microglia Following SNT

The critical role of microglial P2Y12 receptors in neuropathic pain hypersensitivities motivated us to investigate its function in microglial activation following SNT surgery. We have previously shown that ATP induces inward and outward currents, which are known to be mediated by P2X receptors and P2Y receptor-coupled K^+ channels, respectively, and the P2Y12 receptor is the predominant mediator of outward currents in response to ATP (Wu et al., 2007) Using whole-cell patch clamp recording, ATP-induced currents in spinal microglia were recorded at a holding potential of −20mV. Indeed, the outward K^+ currents were almost completely abolished in $P2Y12^{-/-}$ mice (Figure 2A–B). In addition to the use of $P2Y12^{-/-}$ mice, we tested PSB0739 (2 μM), a P2Y12 receptor antagonist (Charolidi et al., 2015), which was also able to significantly reduce the amplitude of the ATP-induced outward current by 50% (n = 5 cells). Consistent with the upregulation of P2Y12 receptors after SNT surgery (Figure 1C), we found that there is a significant increase in ATP-induced outward K^+ currents in ipsilateral microglia (24.46 ± 1.69 pA) compared to contralateral microglia at POD 3 (11.71 ± 1.46 pA) after SNT or those in sham WT mice (14.96 ± 2.25 pA,Figure 2A–B). We also found a similar result at POD 7 (25.74 ± 2.19 pA) after SNT in WT mice.

The potassium current, independent of the response to ATP, is a microglial electrophysiological property and an indicator of the activation status of microglia since microglial electrophysiological properties are known to change during pathological conditions (Avignone et al., 2008; Boucsein et al., 2000; Lyons et al., 2000). Hence, we examined the role of P2Y12 receptors in microglial electrophysiological activation in the spinal dorsal horn after SNT surgery. To this end, we recorded membrane currents in spinal microglial from WT and $P2Y12^{-/-}$ mice following SNT surgery. The cells were held at −60mV and depolarization steps (from −100mV to 80mV) evoked small currents in microglia from sham mice. However, dramatic outwardly rectifying K^+ currents were observed in microglia from the ipsilateral but not microglia from the contralateral spinal dorsal horn at POD 3 after SNT surgery, suggesting the activation of microglia following SNT surgery (Figure 2C–D). Unexpectedly, microglia from POD 7 WT tissues showed

significantly reduced outwardly rectifying K^+ currents compared to microglia from POD 3 WT after SNT surgery, but still significantly more than microglia from sham mice (Figure S6A). These results indicate that microglia in the ipsilateral POD3 peaked in their electrophysiological activation on this day and became less electrophysiologically activated by POD7 after SNT. Next, we examined electrophysiological activation of microglia in P2Y12$^{-/-}$ mice. There was no difference in the basal currents between WT and P2Y12$^{-/-}$ microglia in the dorsal horn (Figure 2C–D). However, we found that SNT-induced outwardly rectifying microglial K^+ currents were largely decreased at POD 3 (Figure 2C–D) and also at POD7 (Figure S6B) in P2Y12$^{-/-}$ mice compared with WT mice, suggesting reduced microglial electrophysiological activation after SNT surgery. Together, these results indicate that P2Y12 receptors mediate ATP-induced K^+ currents and initiates outwardly rectifying K^+ currents, thereby contributing to electrophysiological activation of spinal microglia following SNT.

3.3 P2Y12 Receptors Contribute to Alterations in Static Morphological Properties of Microglia Following SNT

Microglia exhibit astounding morphological activation following SNT, which has traditionally been characterized in terms of its process retraction during activation (Stence et al., 2001). To study the role of P2Y12 in SNT-induced morphological changes, we examined microglia from acute spinal cord slices in WT and P2Y12$^{-/-}$ mice using two photon microscopy. Here, we analyzed the process length of spinal cord microglia in acute slices following SNT surgery. Generally, microglial morphological activation in the ipsilateral dorsal horn was evident at POD 3 but became more widespread by POD 7 (Figure 3A). At both PODs 3 and 7, we selectively monitored microglial morphologies in areas with predominant microglial activation. As expected for microglial activation, microglial process length was significantly reduced at both 3 and 7 days after SNT surgery in the ipsilateral dorsal horn when compared to the contralateral and sham dorsal horn (Figure 3B–C).

Following this initial characterization in WT mice, we performed similar experiments in age-matched P2Y12$^{-/-}$ mice to investigate potential roles of the receptor in SNT-induced microglial activation. Because morphological microglial activation was most robust by POD 7 after SNT surgery, we focused our studies at this time point. In the sham P2Y12$^{-/-}$ dorsal horn, microglial process length was not significantly different from WTs. However, microglial process length were significantly longer in P2Y12$^{-/-}$ dorsal horn than in WT at POD 7 following SNT surgery (Figure 3D).

Furthermore, a Sholl analysis showed similar complexities between microglia in sham WT and P2Y12$^{-/-}$ dorsal horn. The analysis also clearly illustrates that the branching profile of microglia in the POD 7 WT dorsal horn is shifted to the left, an indication of decreased branch complexities, when compared to microglia in sham WT mice. However, 7 days after SNT-induced injury, microglia in the ipsilateral dorsal horn of P2Y12$^{-/-}$ mice exhibited significantly higher complexity, shifted to the right, than those in POD 7 WT mouse tissues (Figure 3E). Data summarized from the Sholl analysis indicates that microglia in the POD 7 P2Y12$^{-/-}$ dorsal horn have significantly more process maximum, longer critical radius and significantly less reduced maximum branch length when compared to cells in the POD 7 WT

dorsal horn. Meanwhile, the Schoenen ramification index also reveals that microglia are more ramified by 27% in the POD7 P2Y12$^{-/-}$ dorsal horn when compared POD 7 WT (Table 1).

Finally, end point voxel analysis was performed as an alternative method to assess microglial structural complexity. We found that even though microglia from sham P2Y12$^{-/-}$ tissues showed significantly lower end point voxels than microglia from sham WT tissues, they displayed greater end point voxels by POD 7 of SNT surgery in the ipsilateral dorsal horn of P2Y12$^{-/-}$ tissues (Figure 3F). These data are consistent with those obtained from the skeleton analysis of process length done on an individual cell-by-cell analysis (Figure 3C–D). Together, these results indicate that microglia lacking P2Y12 receptors show reduced activation morphologically compared with those in WT microglia by POD 7 of SNT surgery.

3.4 P2Y12 Receptors Contribute to Alterations in the Dynamic Morphological Properties of Microglia Following SNT

Microglia are known to play a critical role in tissue surveillance in both the brain and spinal cord (Davalos et al., 2005; Dibaj et al., 2010). Having observed differences in static microglial morphologies between WT and P2Y12$^{-/-}$ mice, we next investigated microglial dynamic motilities following SNT using high resolution two-photon imaging. We began by performing imaging in vivo in the WT spinal cord. Interestingly, we found that the microglial motility index in the ipsilateral dorsal horn was increased compared with those in sham mice at POD 7 following SNT or sham surgery (Figure 4A–B, H). Therefore, microglia have enhanced dynamic surveillance following SNT-induced activation.

Next, we attempted to monitor microglial dynamics in vivo in the spinal cord of P2Y12$^{-/-}$ mice but excessive bleeding from the laminectomy prevented successful imaging. Thus, we resorted to the use of spinal cord slice preparations to examine microglia dynamics. First, we confirmed (as with our observations in vivo) that in WT slices at POD 7 following SNT surgery, microglia exhibited higher motilities (Figure 4C–D, G-H). Then, we examined dynamic morphological properties of microglia after SNT surgery in P2Y12$^{-/-}$ mice. There was no significant difference in microglial motility between WT and P2Y12$^{-/-}$ mice in sham mice. However, SNT-induced increases of microglial motility was significantly reduced in P2Y12$^{-/-}$ tissues (Figure 4E–H). Together, these results suggest that the P2Y12 receptor contributes to microglial tissue surveillance following SNT.

4. DISCUSSION

The major findings of the current study are four-fold. First, we show that microglial P2Y12 receptors are critical in the progression of neuropathic pain using P2Y12$^{-/-}$ mice. Second, we provide the first electrophysiological characterization of microglia during neuropathic pain including evidence for involvement of P2Y12 receptors in certain salient aspects of microglial electrophysiological activation. Third, we present additional evidence for regulation of static microglial morphological characterizations by the P2Y12 receptor during neuropathic pain. Finally, we provide a first description of the dynamic microglia morphological activities induced during neuropathic pain under the control of the P2Y12 receptors. Together, our results indicate that the microglial activation state during

neuropathic pain differs electrophysiologically (peaking at POD 3) and morphologically (progressing at least through POD 7) and highlight an important role for the P2Y12 receptor in microglial activation in the promotion of pain hypersensitivities following peripheral nerve injury.

4.1 P2Y12 Receptor in Neuropathic Pain Hypersensitivities

Previous work (Kobayashi et al., 2008; Kobayashi et al., 2012; Tozaki-Saitoh et al., 2008) has shown that microglial P2Y12 receptors are upregulated at both the mRNA and protein levels following peripheral nerve injury and this upregulation promotes neuropathic pain pathogenesis. We confirmed these results in our initial studies using both male and female $P2Y12^{-/-}$; $CX3CR1^{GFP/+}$ mice. Recently, Sorge et al., 2015 showed that there were differences in the *maintenance* of neuropathic pain in male and female mice (Sorge et al., 2015). However, in our studies that focused on the *initiation* phase (i.e. within the first week) of neuropathic pain, we did not find any such differences. These studies should not be thought to be in conflict since different phases of neuropathic pain were investigated. In addition, even in the maintenance phase of neuropathic pain, microglia still play roles but only secondary to infiltrating T cell in female mice (Sorge et al., 2015).

The precise details of how microglial P2Y12 receptor activation promotes neuropathic pain are not clear. It was suggested that p38 MAPK signaling is critical in this process as pharmacological inhibition of P2Y12 receptors reduced phosphorylated p38 (Kobayashi et al., 2008) even though p38 inhibition did not affect P2Y12 mRNA during neuropathic pain (Kobayashi et al., 2012) suggesting that p38 acts downstream of P2Y12 activation to modulate pain hypersensitivities. Consistently, recent studies suggest that P2Y12 receptors may activate p38 MAPK via Rho-associated coiled-coil-containing protein kinase in microglia after peripheral nerve injury (Tatsumi et al., 2015). Regarding specific mechanisms working upstream of and regulating P2Y12 expression and / or function in microglial surveillance, the transcription factor IRF8 was recently shown to be important in P2Y12-dependent microglial surveillance of isolated cells (Masuda et al., 2014). Since IRF8 is also upregulated during neuropathic and chronic pain with detrimental consequences (Akagi et al., 2014; Masuda et al., 2012), it is reasonable to infer that part of the mechanism by which IRF8 promotes pain is by its regulation of P2Y12 function. Future work will have to be performed to clarify some of these possibilities.

It is also possible (though this has not been extensively investigated) that microglial P2Y12 receptor activation may regulate microglial cytokine production during neuropathic pain. Blockade of P2Y12 receptors on platelets can reduce the release of pro-inflammatory interleukin 1 beta (IL-1β) (Jia et al., 2013), which is released during neuropathic pain and contributes to pain hypersensitivities (Kawasaki et al., 2008; Rutkowski and DeLeo, 2002; Samad et al., 2001). Indeed, there is recent evidence that IL-1β release during neuropathic pain requires P2Y12 receptor activation (Horvath et al., 2014). Thus microglial release of certain cytokines following P2Y12 activation may be a potential route of P2Y12 mediation of pain hypersensitivities.

In addition to spinal cord microglia expressing P2Y12Rs, these receptors have also been found in DRGs (Katagiri et al., 2012; Malin and Molliver, 2010). In the present study, we

did not directly address the role of P2Y12 in the DRG. However, since we used a global P2Y12$^{-/-}$ mice, we cannot rule it out as a potential contributing factor to the P2Y12$^{-/-}$ pain phenotype. This potential role of peripheral P2Y12Rs in neuropathic pain still needs to be further explored.

4.2 P2Y12 Receptor in Electrophysiological and Morphological Activation in Neuropathic Pain

In the current study, without excluding the above-mentioned possibilities (e.g. p38 and cytokine roles), we sought to provide further insights into previously unknown microglial electrophysiological and static / dynamic morphological alterations during the progression of neuropathic pain. Changes in microglial electrophysiology and morphology have been recognized to be hallmarks of microglial activation for several decades (Kettenmann et al., 2011). However, precise descriptions of these fundamental microglial properties have not been investigated during neuropathic pain.

In our study, we found an early activation of these two properties by POD 3 following SNT surgery. The electrophysiological activation of microglia during neuropathic pain was not as dramatic as that in some other pathological contexts such as following seizures (Avignone et al., 2008). While there was a 7 fold increase in current responses to P2Y12 activation following seizures (Avignone et al., 2008), there was only a 1.7 fold increase during neuropathic pain. Similarly, microglial current responses to voltage steps were more dramatic following seizures than following SNT-injury. Though these differences could be a result of the different agonists used to activate the P2Y12 receptor, there is also a possibility that the different injury paradigms may upregulate P2Y12 expression to different degrees. Indeed, although we found an almost 2-fold increase in P2Y12 protein following SNT-injury, seizures induced a 4-fold increase in P2Y12 mRNA (Avignone et al., 2008). These results suggest that modulation of microglial P2Y12 receptors during microglial activation contributes to microglial electrophysiology which may differ depending on the injury/disease context.

Microglial morphologies are important for microglial surveillance. With our end point voxel analysis, we found that microglial process complexity was reduced in the naïve P2Y12$^{-/-}$ spinal cord which was not reported for the naïve P2Y12$^{-/-}$ brain (Haynes et al., 2006). The significance of this difference is not clear since it did not translate to detectable differences in surveillance abilities in the naïve condition. Further studies will be required to determine any such significance exists and whether the difference exists in the brain.

Microglial morphological activation during neuropathic pain has been previously acknowledged (Tsuda et al., 2005; Zhuo et al., 2011). However, our study has now provided further details into the degree of microglial morphological activation including a temporal characterization of microglial process shortening as well as an assessment of microglial process complexity during the first week of neuropathic pain development in mice. In both these morphological features of activation, a deficiency of the P2Y12 ameliorated the SNT-induced morphological changes. A recent study has corroborated some of these findings using a pharmacological approach (Tatsumi et al., 2015). In that study, P2Y12 receptor antagonists were applied following peripheral nerve injury. Under this treatment regimen,

the normally dramatic reduction in microglial process length was inhibited and microglia exhibited much longer primary processes in the injured spinal cord dorsal horn. A previous study (Tozaki-Saitoh et al., 2008) reported no morphological differences between WT and P2Y12$^{-/-}$ tissues at POD 14 after neuropathic pain which seems to contrast with our data. However, our data was generated at POD 7 which is much earlier than the data from that study and may actually suggest that P2Y12Rs delay the morphological transformation of microglia after SNT. Indeed, this is consistent with our data as well since microglial process length is also reduced in P2Y12$^{-/-}$, though less dramatically than that in WT (Figure 3D).

Together, these findings suggest that P2Y12 receptors could be a target for modulating microglial electrophysiological and morphological activation during neuropathic pain. Moreover, whether they also contribute to microglial activation in other CNS injury and / or disease contexts remain to be determined. Our work suggests that such a regulation is possible and since the P2Y12 receptor is a unique marker for microglia in distinction from other CNS and infiltrating cells (Butovsky et al., 2014; Hickman et al., 2013; Moore et al., 2015; Zhang et al., 2014), targeting the receptor may be a unique strategy to improve pain outcomes. However, future studies are needed to address the possible downstream signals that mediate P2Y12 receptor-dependent alterations in microglial electrophysiological and morphological properties during neuropathic pain. Nevertheless, our results highlight the potential therapeutic significance of targeting this receptor in aberrant CNS conditions affected by microglial activation.

4.3 P2Y12 Receptors in Increased Microglial Surveillance in Neuropathic Pain

Microglial surveillance is a fundamental feature of microglial physiology whereby these surveilling cells are proposed to perform homeostatic functions to maintain the health of the CNS (Eyo and Wu, 2013). This constitutive surveillance has been observed in all microglial tissue preparations examined to date including both excised brain slices (Kurpius et al., 2007; Liang et al., 2009; Wu et al., 2007) and in vivo (Davalos et al., 2005; Dibaj et al., 2010; Nimmerjahn et al., 2005). Although the repertoire of the functional significance of this surveillance activity is not clear, it is now widely accepted that it functions at least in part to facilitate regular presumably homeostatic interactions between microglia and neuronal elements to modulate neuronal activity and function (Baalman et al., 2015; Eyo et al., 2014; Li et al., 2012; Tremblay et al., 2010; Wake et al., 2009). A few factors regulating microglial surveillance have been recognized including neuronal activity in general (Fontainhas et al., 2011; Li et al., 2012; Nimmerjahn et al., 2005; Tremblay et al., 2010) as well as through specific molecules including purines (Davalos et al., 2005; Kurpius et al., 2007; Orr et al., 2009) and norepinephrine (Gyoneva and Traynelis, 2013) and diseased conditions such as systemic inflammation (Gyoneva et al., 2014a), Alzheimer's Disease (Krabbe et al., 2013), epilepsy (Eyo et al., 2014), and Parkinson's disease (Gyoneva et al., 2014b). Despite these observations, within the context of neuropathic pain, microglial surveillance has not been investigated. Ours is a first study to show that following SNT-injury, microglial surveillance is increased in slices of the ipsilateral spinal cord dorsal horn. Moreover, although P2Y12 receptors were not found to be critical in the modulation of constitutive microglial surveillance of the spinal cord in P2Y12$^{-/-}$ mouse tissues, a significant component of this SNT-induced increase in microglial surveillance is dependent on this receptor. In line with

this notion, we also found an increased expression of P2Y12 receptors in spinal microglia after SNT.

The immediate functional significance of the observed P2Y12-dependent increase in microglial surveillance during neuropathic pain is not clear. However, because our study and others have shown that microglial P2Y12 receptor function is detrimental during neuropathic pain, it is tempting to speculate that the functional significance of P2Y12 activity (including in the observed increased microglial surveillance) is neurotoxic since the degree of microglial surveillance is positively correlated with the worsened pain phenotypes. During neuropathic pain, microglial P2Y12 receptors may facilitate the altered physical or paracrine engagement of microglia and neurons that may serve to enhance pain hypersensitivities. Indeed, P2Y12 receptors have been found to regulate microglial engulfment of axonal elements following nerve injury in the spinal cord dorsal horn (Maeda et al., 2010).

In conclusion, we have demonstrated a role for microglial P2Y12 receptor function in neuropathic pain. This role has been shown at both electrophysiological, morphological that indicate important regulation of microglial activity by this receptor. Because the P2Y12 receptor participates in the release of various cytokines that promote inflammatory and neuropathic pain as well as the availability of potent P2Y12 antagonists that can reduce chronic inflammatory and neuropathic pain (Horvath et al., 2014), our results suggest that further understanding P2Y12 function in neuropathic pain contexts could help in the targeted treatment of pain management especially since these receptors are unique to microglia in the CNS and regulate microglial inflammatory responses (Moore et al., 2015).

Supplementary Material

Refer to Web version on PubMed Central for supplementary material.

Acknowledgments

This work is supported by National Institute of Health (R01NS088627, T32ES007148), New Jersey Commission on Spinal Cord Research (CSCR15ERG015), Target Validation Grant from Michael J. Fox Foundation, and National Natural Science Foundation of China (No. 81200857). We thank all members of Wu lab at Rutgers for insightful discussions.

References

Akagi T, Matsumura Y, Yasui M, Minami E, Inoue H, Masuda T, Tozaki-Saitoh H, Tamura T, Mizumura K, Tsuda M, Kiyama H, Inoue K. Interferon regulatory factor 8 expressed in microglia contributes to tactile allodynia induced by repeated cold stress in rodents. J Pharmacol Sci. 2014; 126:172–176. [PubMed: 25273233]

Andre P, Delaney SM, LaRocca T, Vincent D, DeGuzman F, Jurek M, Koller B, Phillips DR, Conley PB. P2Y12 regulates platelet adhesion/activation, thrombus growth, and thrombus stability in injured arteries. J Clin Invest. 2003; 112:398–406. [PubMed: 12897207]

Avignone E, Ulmann L, Levavasseur F, Rassendren F, Audinat E. Status epilepticus induces a particular microglial activation state characterized by enhanced purinergic signaling. J Neurosci. 2008; 28:9133–9144. [PubMed: 18784294]

Baalman K, Marin MA, Ho TS, Godoy M, Cherian L, Robertson C, Rasband MN. Axon initial segment-associated microglia. J Neurosci. 2015; 35:2283–2292. [PubMed: 25653382]

Baron R. Mechanisms of disease: neuropathic pain--a clinical perspective. Nat Clin Pract Neurol. 2006; 2:95–106. [PubMed: 16932531]

Boucsein C, Kettenmann H, Nolte C. Electrophysiological properties of microglial cells in normal and pathologic rat brain slices. Eur J Neurosci. 2000; 12:2049–2058. [PubMed: 10886344]

Butovsky O, Jedrychowski MP, Moore CS, Cialic R, Lanser AJ, Gabriely G, Koeglsperger T, Dake B, Wu PM, Doykan CE, Fanek Z, Liu L, Chen Z, Rothstein JD, Ransohoff RM, Gygi SP, Antel JP, Weiner HL. Identification of a unique TGF-beta-dependent molecular and functional signature in microglia. Nat Neurosci. 2014; 17:131–143. [PubMed: 24316888]

Charolidi N, Schilling T, Eder C. Microglial Kv1.3 Channels and P2Y12 Receptors Differentially Regulate Cytokine and Chemokine Release from Brain Slices of Young Adult and Aged Mice. PLoS One. 2015; 10:e0128463. [PubMed: 26011191]

Chung JM, Kim HK, Chung K. Segmental spinal nerve ligation model of neuropathic pain. Methods Mol Med. 2004; 99:35–45. [PubMed: 15131327]

Clark AK, Old EA, Malcangio M. Neuropathic pain and cytokines: current perspectives. J Pain Res. 2013; 6:803–814. [PubMed: 24294006]

Davalos D, Grutzendler J, Yang G, Kim JV, Zuo Y, Jung S, Littman DR, Dustin ML, Gan WB. ATP mediates rapid microglial response to local brain injury in vivo. Nat Neurosci. 2005; 8:752–758. [PubMed: 15895084]

Davalos D, Lee JK, Smith WB, Brinkman B, Ellisman MH, Zheng B, Akassoglou K. Stable in vivo imaging of densely populated glia, axons and blood vessels in the mouse spinal cord using two-photon microscopy. J Neurosci Methods. 2008; 169:1–7. [PubMed: 18192022]

Dibaj P, Nadrigny F, Steffens H, Scheller A, Hirrlinger J, Schomburg ED, Neusch C, Kirchhoff F. NO mediates microglial response to acute spinal cord injury under ATP control in vivo. Glia. 2010; 58:1133–1144. [PubMed: 20468054]

Eyo U, Dailey ME. Effects of oxygen-glucose deprivation on microglial mobility and viability in developing mouse hippocampal tissues. Glia. 2012; 60:1747–1760. [PubMed: 22847985]

Eyo UB, Gu N, De S, Dong H, Richardson JR, Wu LJ. Modulation of microglial process convergence toward neuronal dendrites by extracellular calcium. J Neurosci. 2015; 35:2417–2422. [PubMed: 25673836]

Eyo UB, Peng J, Swiatkowski P, Mukherjee A, Bispo A, Wu LJ. Neuronal Hyperactivity Recruits Microglial Processes via Neuronal NMDA Receptors and Microglial P2Y12 Receptors after Status Epilepticus. J Neurosci. 2014; 34:10528–10540. [PubMed: 25100587]

Eyo UB, Wu LJ. Bi-directional microglia-neuron communication in the healthy brain. Neural plasticity. 2013; 2013:456857. [PubMed: 24078884]

Ferrini F, De Koninck Y. Microglia control neuronal network excitability via BDNF signalling. Neural Plast. 2013; 2013:429815. [PubMed: 24089642]

Fontainhas AM, Wang M, Liang KJ, Chen S, Mettu P, Damani M, Fariss RN, Li W, Wong WT. Microglial morphology and dynamic behavior is regulated by ionotropic glutamatergic and GABAergic neurotransmission. PLoS One. 2011; 6:e15973. [PubMed: 21283568]

Gu N, Niu JY, Liu WT, Sun YY, Liu S, Lv Y, Dong HL, Song XJ, Xiong LZ. Hyperbaric oxygen therapy attenuates neuropathic hyperalgesia in rats and idiopathic trigeminal neuralgia in patients. Eur J Pain. 2012; 16:1094–1105. [PubMed: 22354664]

Gyoneva S, Davalos D, Biswas D, Swanger SA, Garnier-Amblard E, Loth F, Akassoglou K, Traynelis SF. Systemic inflammation regulates microglial responses to tissue damage in vivo. Glia. 2014a; 62:1345–1360. [PubMed: 24807189]

Gyoneva S, Shapiro L, Lazo C, Garnier-Amblard E, Smith Y, Miller GW, Traynelis SF. Adenosine A2A receptor antagonism reverses inflammation-induced impairment of microglial process extension in a model of Parkinson's disease. Neurobiol Dis. 2014b; 67:191–202. [PubMed: 24632419]

Gyoneva S, Traynelis SF. Norepinephrine modulates the motility of resting and activated microglia via different adrenergic receptors. J Biol Chem. 2013; 288:15291–15302. [PubMed: 23548902]

Haynes SE, Hollopeter G, Yang G, Kurpius D, Dailey ME, Gan WB, Julius D. The P2Y12 receptor regulates microglial activation by extracellular nucleotides. Nat Neurosci. 2006; 9:1512–1519. [PubMed: 17115040]

Hickman SE, Kingery ND, Ohsumi TK, Borowsky ML, Wang LC, Means TK, El Khoury J. The microglial sensome revealed by direct RNA sequencing. Nat Neurosci. 2013; 16:1896–1905. [PubMed: 24162652]

Horvath G, Goloncser F, Csolle C, Kiraly K, Ando RD, Baranyi M, Kovanyi B, Mate Z, Hoffmann K, Algaier I, Baqi Y, Muller CE, Von Kugelgen I, Sperlagh B. Central P2Y12 receptor blockade alleviates inflammatory and neuropathic pain and cytokine production in rodents. Neurobiol Dis. 2014; 70:162–178. [PubMed: 24971933]

Inoue K, Tsuda M. P2X4 receptors of microglia in neuropathic pain. CNS Neurol Disord Drug Targets. 2012; 11:699–704. [PubMed: 22963435]

Jia LX, Qi GM, Liu O, Li TT, Yang M, Cui W, Zhang WM, Qi YF, Du J. Inhibition of platelet activation by clopidogrel prevents hypertension-induced cardiac inflammation and fibrosis. Cardiovasc Drugs Ther. 2013; 27:521–530. [PubMed: 23887740]

Johnston IN, Milligan ED, Wieseler-Frank J, Frank MG, Zapata V, Campisi J, Langer S, Martin D, Green P, Fleshner M, Leinwand L, Maier SF, Watkins LR. A role for proinflammatory cytokines and fractalkine in analgesia, tolerance, and subsequent pain facilitation induced by chronic intrathecal morphine. J Neurosci. 2004; 24:7353–7365. [PubMed: 15317861]

Jung S, Aliberti J, Graemmel P, Sunshine MJ, Kreutzberg GW, Sher A, Littman DR. Analysis of fractalkine receptor CX(3)CR1 function by targeted deletion and green fluorescent protein reporter gene insertion. Mol Cell Biol. 2000; 20:4106–4114. [PubMed: 10805752]

Katagiri A, Shinoda M, Honda K, Toyofuku A, Sessle BJ, Iwata K. Satellite glial cell P2Y12 receptor in the trigeminal ganglion is involved in lingual neuropathic pain mechanisms in rats. Mol Pain. 2012; 8:23. [PubMed: 22458630]

Kawasaki Y, Zhang L, Cheng JK, Ji RR. Cytokine mechanisms of central sensitization: distinct and overlapping role of interleukin-1beta, interleukin-6, and tumor necrosis factor-alpha in regulating synaptic and neuronal activity in the superficial spinal cord. J Neurosci. 2008; 28:5189–5194. [PubMed: 18480275]

Kettenmann H, Hanisch UK, Noda M, Verkhratsky A. Physiology of microglia. Physiol Rev. 2011; 91:461–553. [PubMed: 21527731]

Kim D, You B, Jo EK, Han SK, Simon MI, Lee SJ. NADPH oxidase 2-derived reactive oxygen species in spinal cord microglia contribute to peripheral nerve injury-induced neuropathic pain. Proc Natl Acad Sci U S A. 2010; 107:14851–14856. [PubMed: 20679217]

Kobayashi K, Yamanaka H, Fukuoka T, Dai Y, Obata K, Noguchi K. P2Y12 receptor upregulation in activated microglia is a gateway of p38 signaling and neuropathic pain. J Neurosci. 2008; 28:2892–2902. [PubMed: 18337420]

Kobayashi K, Yamanaka H, Yanamoto F, Okubo M, Noguchi K. Multiple P2Y subtypes in spinal microglia are involved in neuropathic pain after peripheral nerve injury. Glia. 2012; 60:1529–1539. [PubMed: 22736439]

Krabbe G, Halle A, Matyash V, Rinnenthal JL, Eom GD, Bernhardt U, Miller KR, Prokop S, Kettenmann H, Heppner FL. Functional impairment of microglia coincides with Beta-amyloid deposition in mice with Alzheimer-like pathology. PLoS One. 2013; 8:e60921. [PubMed: 23577177]

Kurpius D, Nolley EP, Dailey ME. Purines induce directed migration and rapid homing of microglia to injured pyramidal neurons in developing hippocampus. Glia. 2007; 55:873–884. [PubMed: 17405148]

Li Y, Du XF, Liu CS, Wen ZL, Du JL. Reciprocal regulation between resting microglial dynamics and neuronal activity in vivo. Dev Cell. 2012; 23:1189–1202. [PubMed: 23201120]

Liang KJ, Lee JE, Wang YD, Ma W, Fontainhas AM, Fariss RN, Wong WT. Regulation of dynamic behavior of retinal microglia by CX3CR1 signaling. Invest Ophthalmol Vis Sci. 2009; 50:4444–4451. [PubMed: 19443728]

Liu F, Yuan H. Role of glia in neuropathic pain. Front Biosci (Landmark Ed). 2014; 19:798–807. [PubMed: 24389224]

Lyons SA, Pastor A, Ohlemeyer C, Kann O, Wiegand F, Prass K, Knapp F, Kettenmann H, Dirnagl U. Distinct physiologic properties of microglia and blood-borne cells in rat brain slices after

permanent middle cerebral artery occlusion. J Cereb Blood Flow Metab. 2000; 20:1537–1549. [PubMed: 11083228]

Maeda M, Tsuda M, Tozaki-Saitoh H, Inoue K, Kiyama H. Nerve injury-activated microglia engulf myelinated axons in a P2Y12 signaling-dependent manner in the dorsal horn. Glia. 2010; 58:1838–1846. [PubMed: 20665560]

Malin SA, Molliver DC. Gi- and Gq-coupled ADP (P2Y) receptors act in opposition to modulate nociceptive signaling and inflammatory pain behavior. Mol Pain. 2010; 6:21. [PubMed: 20398327]

Masuda T, Nishimoto N, Tomiyama D, Matsuda T, Tozaki-Saitoh H, Tamura T, Kohsaka S, Tsuda M, Inoue K. IRF8 is a transcriptional determinant for microglial motility. Purinergic Signal. 2014; 10:515–521. [PubMed: 24798612]

Masuda T, Tsuda M, Yoshinaga R, Tozaki-Saitoh H, Ozato K, Tamura T, Inoue K. IRF8 is a critical transcription factor for transforming microglia into a reactive phenotype. Cell Rep. 2012; 1:334–340. [PubMed: 22832225]

Moore CS, Ase AR, Kinsara A, Rao VT, Michell-Robinson M, Leong SY, Butovsky O, Ludwin SK, Seguela P, Bar-Or A, Antel JP. P2Y12 expression and function in alternatively activated human microglia. Neurol Neuroimmunol Neuroinflamm. 2015; 2:e80. [PubMed: 25821842]

Morrison HW, Filosa JA. A quantitative spatiotemporal analysis of microglia morphology during ischemic stroke and reperfusion. J Neuroinflammation. 2013; 10:4. [PubMed: 23311642]

Nimmerjahn A, Kirchhoff F, Helmchen F. Resting microglial cells are highly dynamic surveillants of brain parenchyma in vivo. Science. 2005; 308:1314–1318. [PubMed: 15831717]

Old EA, Clark AK, Malcangio M. The role of glia in the spinal cord in neuropathic and inflammatory pain. Handb Exp Pharmacol. 2015; 227:145–170. [PubMed: 25846618]

Orr AG, Orr AL, Li XJ, Gross RE, Traynelis SF. Adenosine A(2A) receptor mediates microglial process retraction. Nat Neurosci. 2009; 12:872–878. [PubMed: 19525944]

Rutkowski MD, DeLeo JA. The Role of Cytokines in the Initiation and Maintenance of Chronic Pain. Drug News Perspect. 2002; 15:626–632. [PubMed: 12677247]

Samad TA, Moore KA, Sapirstein A, Billet S, Allchorne A, Poole S, Bonventre JV, Woolf CJ. Interleukin-1beta-mediated induction of Cox-2 in the CNS contributes to inflammatory pain hypersensitivity. Nature. 2001; 410:471–475. [PubMed: 11260714]

Sorge RE, Mapplebeck JC, Rosen S, Beggs S, Taves S, Alexander JK, Martin LJ, Austin JS, Sotocinal SG, Chen D, Yang M, Shi XQ, Huang H, Pillon NJ, Bilan PJ, Tu Y, Klip A, Ji RR, Zhang J, Salter MW, Mogil JS. Different immune cells mediate mechanical pain hypersensitivity in male and female mice. Nat Neurosci. 2015; 18:1081–1083. [PubMed: 26120961]

Staniland AA, Clark AK, Wodarski R, Sasso O, Maione F, D'Acquisto F, Malcangio M. Reduced inflammatory and neuropathic pain and decreased spinal microglial response in fractalkine receptor (CX3CR1) knockout mice. J Neurochem. 2010; 114:1143–1157. [PubMed: 20524966]

Stence N, Waite M, Dailey ME. Dynamics of microglial activation: a confocal time-lapse analysis in hippocampal slices. Glia. 2001; 33:256–266. [PubMed: 11241743]

Tatsumi E, Yamanaka H, Kobayashi K, Yagi H, Sakagami M, Noguchi K. RhoA/ROCK pathway mediates p38 MAPK activation and morphological changes downstream of P2Y12/13 receptors in spinal microglia in neuropathic pain. Glia. 2015; 63:216–228. [PubMed: 25130721]

Tozaki-Saitoh H, Tsuda M, Miyata H, Ueda K, Kohsaka S, Inoue K. P2Y12 receptors in spinal microglia are required for neuropathic pain after peripheral nerve injury. J Neurosci. 2008; 28:4949–4956. [PubMed: 18463248]

Trang T, Beggs S, Salter MW. ATP receptors gate microglia signaling in neuropathic pain. Exp Neurol. 2012; 234:354–361. [PubMed: 22116040]

Tremblay ME, Lowery RL, Majewska AK. Microglial interactions with synapses are modulated by visual experience. PLoS Biol. 2010; 8:e1000527. [PubMed: 21072242]

Tsuda M, Inoue K, Salter MW. Neuropathic pain and spinal microglia: a big problem from molecules in "small" glia. Trends Neurosci. 2005; 28:101–107. [PubMed: 15667933]

Tsuda M, Masuda T, Tozaki-Saitoh H, Inoue K. Microglial regulation of neuropathic pain. J Pharmacol Sci. 2013; 121:89–94. [PubMed: 23337437]

Vallejo R, Tilley DM, Vogel L, Benyamin R. The role of glia and the immune system in the development and maintenance of neuropathic pain. Pain Pract. 2010; 10:167–184. [PubMed: 20384965]

Wake H, Moorhouse AJ, Jinno S, Kohsaka S, Nabekura J. Resting microglia directly monitor the functional state of synapses in vivo and determine the fate of ischemic terminals. J Neurosci. 2009; 29:3974–3980. [PubMed: 19339593]

Wu LJ, Vadakkan KI, Zhuo M. ATP-induced chemotaxis of microglial processes requires P2Y receptor-activated initiation of outward potassium currents. Glia. 2007; 55:810–821. [PubMed: 17357150]

Wu LJ, Wu G, Akhavan Sharif MR, Baker A, Jia Y, Fahey FH, Luo HR, Feener EP, Clapham DE. The voltage-gated proton channel Hv1 enhances brain damage from ischemic stroke. Nat Neurosci. 2012; 15:565–573. [PubMed: 22388960]

Zhang Y, Chen K, Sloan SA, Bennett ML, Scholze AR, O'Keeffe S, Phatnani HP, Guarnieri P, Caneda C, Ruderisch N, Deng S, Liddelow SA, Zhang C, Daneman R, Maniatis T, Barres BA, Wu JQ. An RNA-sequencing transcriptome and splicing database of glia, neurons, and vascular cells of the cerebral cortex. J Neurosci. 2014; 34:11929–11947. [PubMed: 25186741]

Zhuo M, Wu G, Wu LJ. Neuronal and microglial mechanisms of neuropathic pain. Mol Brain. 2011; 4:31. [PubMed: 21801430]

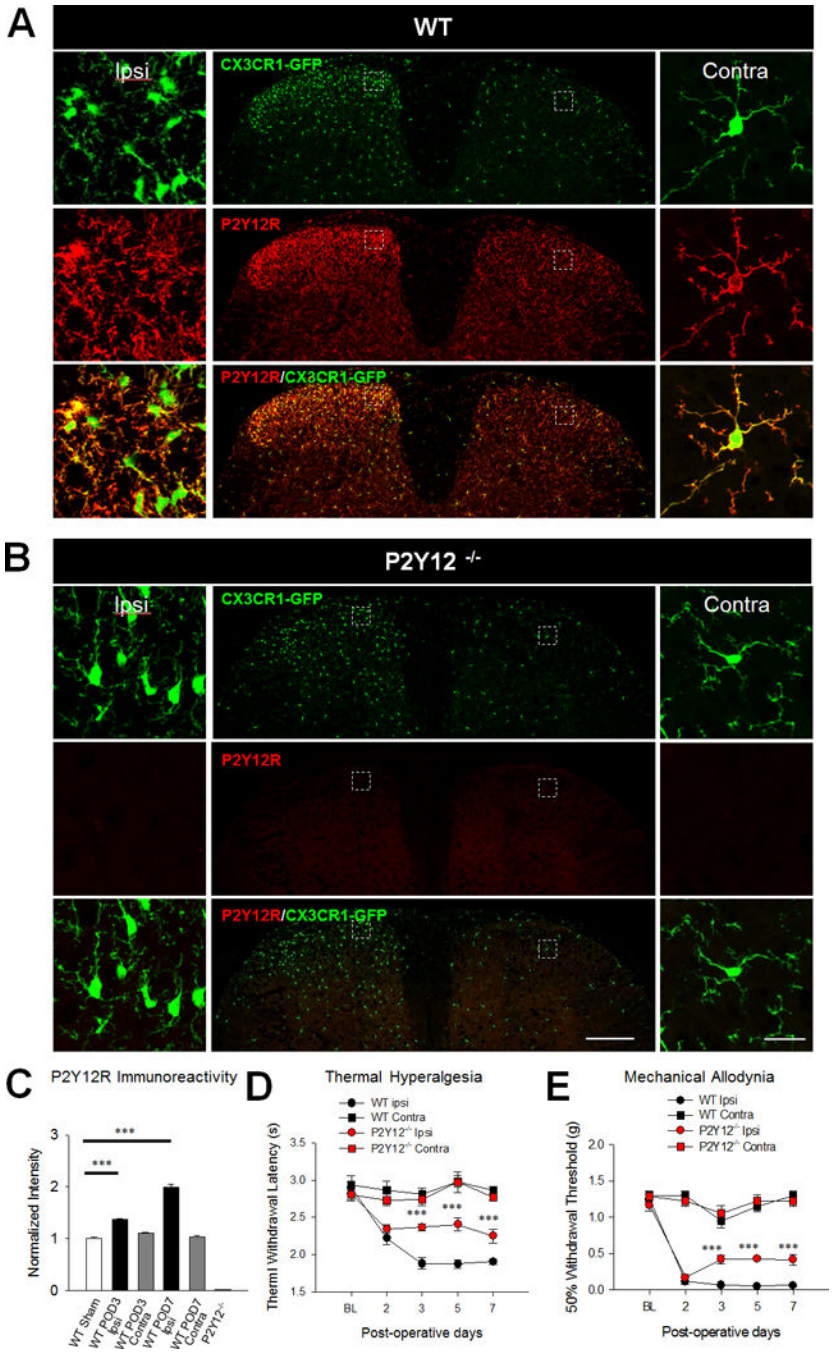

Figure 1. Microglial P2Y12 Receptors Are Upregulated to Promote Neuropathic Pain

A–B, Representative low and high magnification confocal images of both the ipsilateral and contralateral dorsal horns of the spinal cord at post-operative day (POD) 7 following spinal nerve transection (SNT). Microglia are shown in green in CX3CR1$^{GFP/+}$ mice in both WT and P2Y12$^{-/-}$ tissues and P2Y12 immunoreactivity is shown in red. Scale bar is 200 μm and 20 μm for lower and higher magnification images, respectively. **C**, Quantified P2Y12 immunoreactivity is higher in the ipsilateral compared to the contralateral dorsal horn in WT mice but remains absent in the dorsal horn of P2Y12$^{-/-}$ mice at POD 7. n=4 mice per group.

Data are shown as mean ± SEM. *** P < 0.001. **D–E**, Pain hypersensitivities including thermal hyperalgesia (**D**) and mechanical allodynia (**E**) are reduced in P2Y12$^{-/-}$ mice compared to WT mice. n=7–8 per group. Data are shown as mean ± SEM. *** P < 0.001.

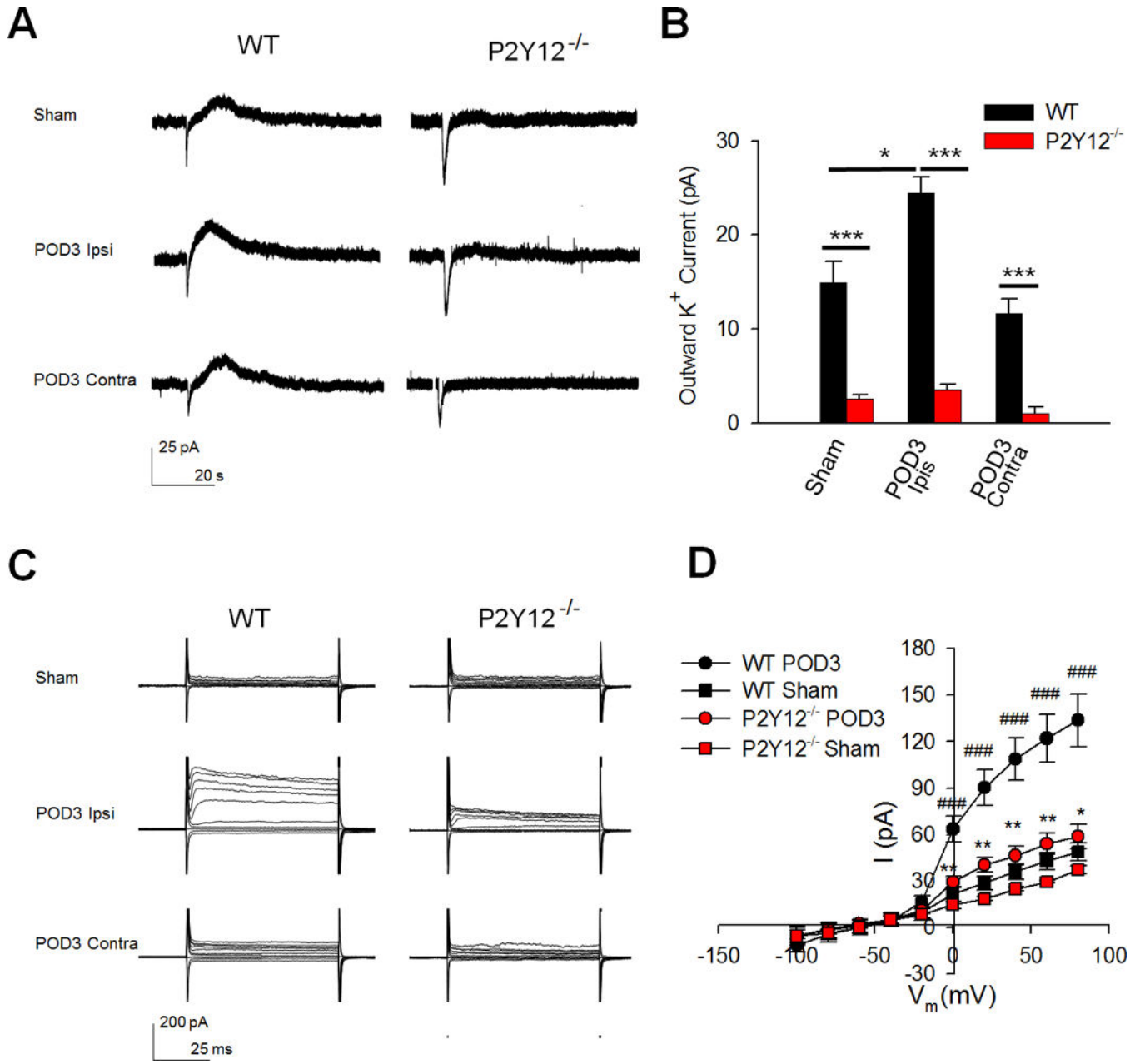

Figure 2. P2Y12 Receptors Limit Microglial Electrophysiological Activation during Neuropathic Pain

A–B, Representative tracings showing (**A**) and quantified summaries of (**B**) outward currents in response to ATP (1mM) puff application to microglia from sham and SNT-surgery WT and P2Y12$^{-/-}$ mice. n=3–5 cells per group. Data are shown as mean ± SEM. * P < 0.05; *** P < 0.001. **C–D**, Representative tracings showing (**C**) and quantified summaries of (**D**) depolarization steps from −100mV to 80mV in microglia from sham and SNT-surgery WT and P2Y12$^{-/-}$ mice. n=10 cells for WT Sham group, n=17 cells for WT POD3 group, n=3 cells for P2Y12$^{-/-}$ Sham group, n=11 cells for P2Y12$^{-/-}$ POD3 group. Data are shown as mean ± SEM. *P < 0.05; **P < 0.01; *** P < 0.001 compared with WT POD 3; ###P < 0.001 compared with WT Sham.

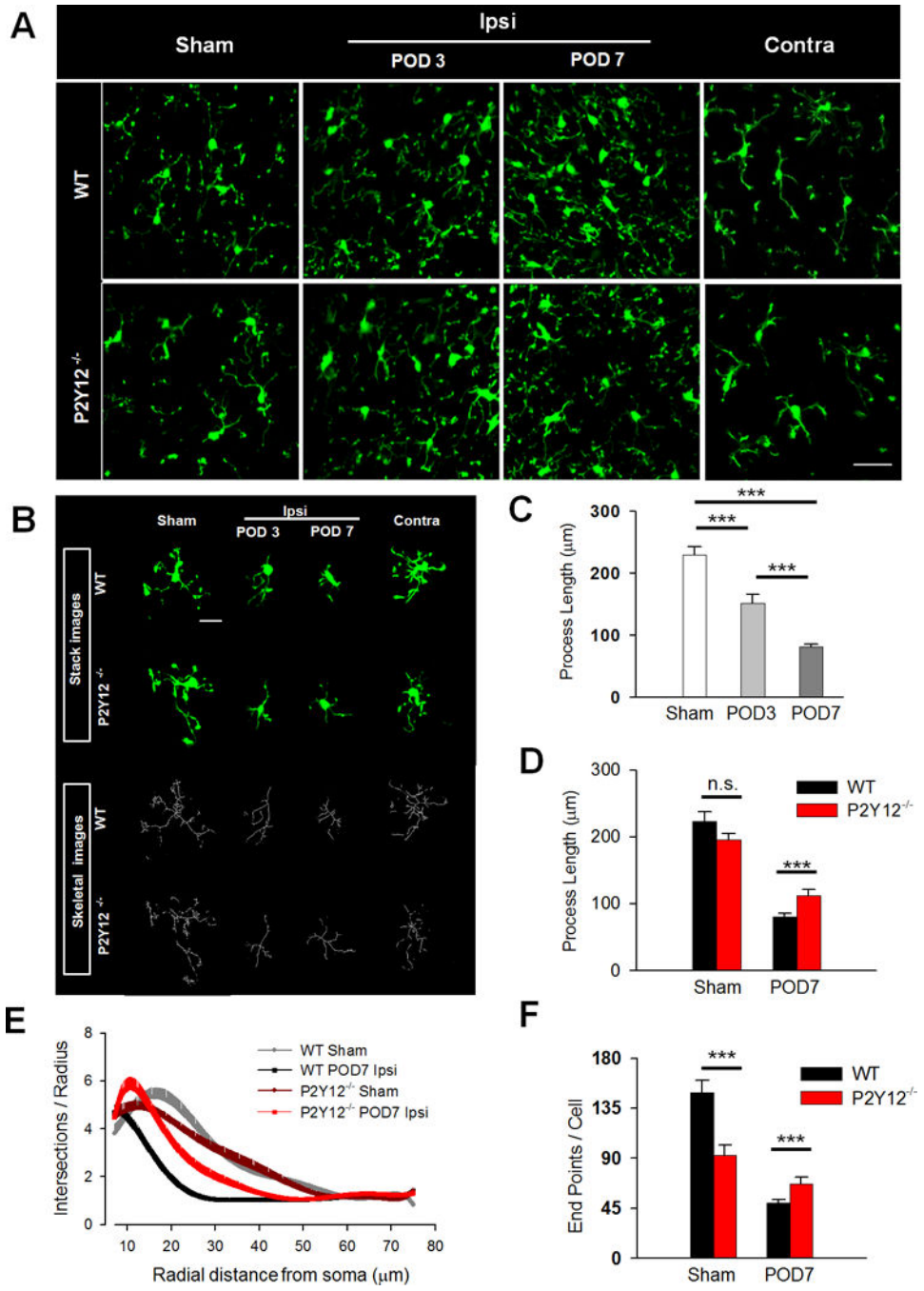

Figure 3. P2Y12 Receptors Limit Microglial Morphological Activation during Neuropathic Pain

A, Representative two-photon z-stack images of GFP-expressing microglia in the spinal cord dorsal horn of sham (left) ipsilateral (left and right center) and contralateral (right) dorsal horn from WT (top) and P2Y12$^{-/-}$ (bottom) tissue slices. Scale bar is 200 μm. **B**, Representative raw (green) and transformed skeletal (gray) images from sham (left) ipsilateral (left and right center) and contralateral (right) dorsal horn from WT (top) and P2Y12$^{-/-}$ (bottom) tissues. Scale bar is 20 μm. **C**, Quantification of microglial process length in WT sham as well POD 3 and 7 following SNT surgery showing progressive

shortening of process lengths. n=6–9 slices per group (from 3 mice). Data are shown as mean ± SEM. *** P < 0.001. **D**, Quantification of microglial process length in WT and P2Y12$^{-/-}$ microglial at POD 7 following SNT surgery in WT and P2Y12$^{-/-}$ tissues. n=8–11 slices per group (form 4 mice). Data are shown as mean ± SEM. *** P < 0.001. **E–F**, Sholl (**E**) and endpoint voxel (**F**) analysis of microglia from WT and P2Y12$^{-/-}$ tissues in the sham and at POD 7 following SNT surgery. n=14–25 cells per group from 5–7 mice for Sholl analysis and n=8–11 slices per group from 4 mice for endpoint voxel analysis. Data are shown as mean ± SEM. n.s., no significance. * P < 0.05; *** P < 0.001

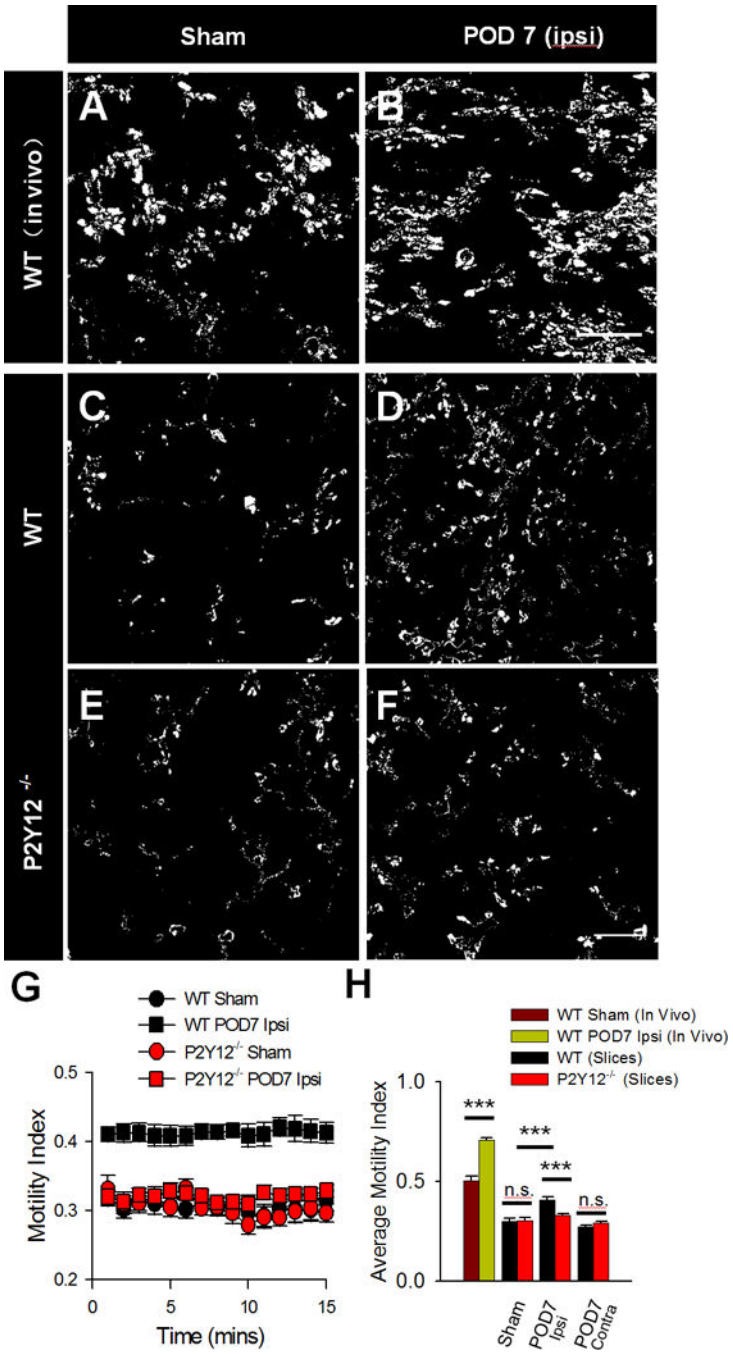

Figure 4. P2Y12 Receptors Limit Microglial Dynamics during Neuropathic Pain

A–F, Representative difference images used to quantify microglial motility indices of microglia from WT mice in vivo (**A–B**) WT slices (**C–D**) and P2Y12$^{-/-}$ slices (**E–F**) under sham conditions (left), and POD 7 following SNT surgery in the ipsilateral dorsal horn. Scale bar is 25 μm. **G–H**, Quantification of microglial motility indices from WT and P2Y12$^{-/-}$ slices during 15 minute long imaging sessions represented as a summary through time (**G**) as well as an average for each condition (**H**). n=4–6 mice per group for in vivo

images and n=6–11 slices from 3–6 mice per group for slices images. Data are shown as mean ± SEM. n.s., no significance. *** $P < 0.001$.

Table 1

Sholl Analysis Data Summary

	WT Sham	P2Y12$^{-/-}$ Sham	WT POD7	P2Y12$^{-/-}$ POD7
Process Maximum (Nm)	10.06 ± 0.57	8.64 ± 0.45	7.84 ± 0.39$^{\#\#\#}$	9.91 ± 0.53**
Critical Radius(rc : um)	16.51 ± 1.81	14.68 ± 1.91	8.95 ± 0.45$^{\#\#\#}$	11.00 ± 0.75$^{*\#\#\#}$
Maximum Branch Length (um)	41.94 ± 2.19	42.71 ± 2.09	20.44 ± 0.86$^{\#\#\#}$	28.63 ±1.68$^{***\#\#\#\dagger\dagger\dagger}$
Number of Primary Branches (Np)	4.27 ± 0.38	4.48 ± 0.49	4.69 ± 0.38	4.61 ± 0.39
Schoenen Ramification Index (Nm/Np)	2.81 ± 0.31	2.12 ± 0.17	1.89 ± 0.14$^{\#\#\#}$	2.40 ± 0.19*
n = Cells/Animal	16/5	14/6	25/5	23/7

Note:

*<0.05,

**<0.01,

***<0.001 Compared with WT POD7;

$^{\#}$<0.05,

$^{\#\#}$<0.01,

$^{\#\#\#}$<0.001 Compared with WT Sham;

†<0.05,

††<0.01,

†††<0.001 Compared with P2Y12$^{-/-}$ Sham.